Available online at www.sciencedirect.com
SCIENCE DIRECT®
PERGAMON
Deep-Sea Research I 50 (2003) 1023–1042
DEEP-SEA RESEARCH PART I
www.elsevier.com/locate/dsr

# The inorganic carbon system in the coastal upwelling region west of Vancouver Island, Canada

Debby Ianson[a,*], Susan E. Allen[a], Shannon L. Harris[a], Kristin J. Orians[a], Diana E. Varela[a,b], Chi S. Wong[c]

[a] *Oceanography, Department of Earth and Ocean Sciences, University of British Columbia, Vancouver, BC, Canada V6T 1Z4*
[b] *Department of Biological Sciences, Simon Fraser University, Burnaby, BC, Canada V5A 1S6*
[c] *Institute of Ocean Sciences, P.O. Box 6000, Sidney, BC, Canada V8L 4B2*

Received 9 December 2002; accepted 20 May 2003

**Abstract**

We present inorganic carbon data from the coastal upwelling region west of Vancouver Island, Canada (~48.5°N, 126°W) directly after an upwelling event and during summer downwelling in July 1998. The inner-shelf buoyancy current, the outer-shelf and the slope regions are contrasted for both wind regimes (up- and downwelling). Results show strong biological drawdown of the partial pressure of carbon dioxide ($pCO_2$) in response to upwelling over the outer-shelf. In contrast, measured $pCO_2$ is exceptionally high ($pCO_2 > 1000$ ppm) in the inner-shelf current, where biological uptake of carbon is consistently large. The biological C:N uptake ratio appears to increase when nitrogen becomes limiting (during downwelling), while the POC:PON ratio is relatively constant (slightly lower than the Redfield ratio) suggesting that excess carbon uptake does not go into the POC pool. As expected, large cells dominate where measured primary productivity is greatest. Sub-surface inorganic carbon (and $pCO_2$) is high over the shelf. We suggest that carbon concentrations may be higher in coastal waters because of remineralization associated with high productivity that is confined to a smaller volume of water by bathymetry. At the coast these sub-surface concentrations are more efficiently mixed into the surface (especially during winter) relative to deeper offshore regions. Thus, despite high primary production, coastal waters may not aid in sequestration of atmospheric carbon.


*Keywords:* Continental shelf; Gas flux; Nutrient cycling; Carbon; Nitrogen; Field measurements; Vancouver Island; British Columbia

## 1. Introduction

Vertically exported fluxes of organic carbon (as estimated from *f*-ratios (Dugdale and Goering, 1967)) are disproportionately large over continental margins relative to the open ocean (Eppley and Peterson, 1979; Harrison et al., 1987). Despite the small surface area of these regions, they are dynamic and likely to be important to the global carbon budget. However, few inorganic carbon data have been collected in the coastal ocean.

Coastal upwelling brings intermediate depth water to the surface (Smith, 1994). Thus, coastal upwelling regions have the potential to ventilate inorganic carbon and could be a source of carbon

*Corresponding author.
*E-mail address:* iansond@pac.dfo-mpo.gc.ca (D. Ianson).

0967-0637/03/$ - see front matter 
doi:10.1016/S0967-0637(03)00114-6

dioxide to the atmosphere (Christensen, 1994). However, biologically limiting nutrients (such as nitrogen) are also brought to the surface during upwelling and they allow high, diatom-based, primary production (PP) (Hutchings et al., 1994). The drawdown of inorganic carbon associated with this high production has been shown to cause low surface partial pressures of carbon dioxide ($pCO_2$) off the coasts of Peru and California (Friederich et al., 1994; Simpson, 1986; Simpson and Zirino, 1980). This drawdown has led some to suggest that coastal upwelling regions may be a significant sink of atmospheric $CO_2$.

Other studies have suggested that some non-upwelling coastal systems may also absorb $CO_2$ from the atmosphere by biological drawdown in the surface ocean. For example, Codispoti et al. (1986) observed intense spring drawdown of $pCO_2$ in the Bering Sea. The North Sea was also shown to be a net sink of atmospheric $CO_2$ during the summer (Kempe and Pegler, 1991). Data reported from the China Sea by Tsunogai et al. (1999) suggest that this region is a net sink of atmospheric $CO_2$ even during the winter. These results have been extrapolated in a global modelling study to imply that the world's coastal oceans are responsible for a substantial net uptake of carbon (Yool and Fasham, 2001).

There is an additional mechanism that would significantly enhance biological $pCO_2$ drawdown in the surface ocean. Phytoplankton may take up dissolved inorganic carbon (DIC) in excess relative to limiting nutrients, such as nitrogen (i.e., non-Redfield C:N uptake, Redfield et al., 1963). As a result, the organic matter exported from the upper ocean layer may be enriched in carbon relative to nitrogen (thus sequestering more carbon than the nitrogen-based $f$-ratio suggests), an issue of great biogeochemical significance. This elevated C:N uptake has been observed in the North Atlantic, over Georges Bank (Sambrotto et al., 1993) and in the Bering Sea (Codispoti et al., 1986). Similarly, Goldman et al. (1992) and Richardson and Cullen (1995) have found carbon and nitrogen uptake by marine diatoms to be uncoupled in lab experiments, where photosynthesis occurred in the absence of nutrient uptake.

We report inorganic carbon data from the coastal upwelling region west of southern Vancouver Island following an upwelling event and during a period of summer downwelling and relaxation conditions. Although not as shallow, the continental shelf in this region is generally wider than off the Oregon, Californian and Peruvian coasts (20–30 km on lines D and G) and almost as broad as the Northwest African shelf in some areas (40–50 km on lines A and C) (Fig. 1). Upwelling off Vancouver Island is driven both by local wind forcing and by wind forcing further south along the Oregon and Californian coasts, connected to this region via shelf waves (Freeland and Denman, 1982). In addition, a buoyancy current (the Vancouver Island Coastal Current, VICC) flows northward throughout the year over the inner-shelf along the southern coast of Vancouver Island (Freeland et al., 1984; Hickey et al., 1991) (Fig. 2). The current is fed by low density (fresher) surface outflow from the Juan de Fuca Strait (this fresh water originates in the run-off from the coastal mountains on the mainland) and by local fresh water runoff from Vancouver Island. The low density surface water creates a horizontal pressure gradient that interacts with the

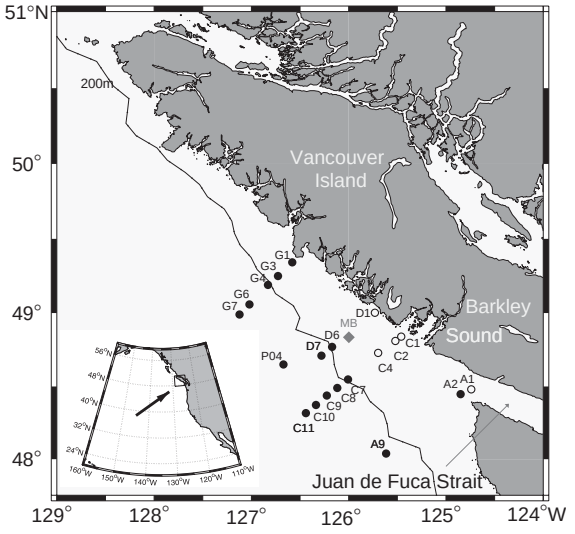


Fig. 1. A map of all stations sampled. MB marks the location of the meteorological buoy. The Juan de Fuca Strait is the source of the Vancouver Island Coastal Current. The 200 m depth contour runs approximately along the shelf break.

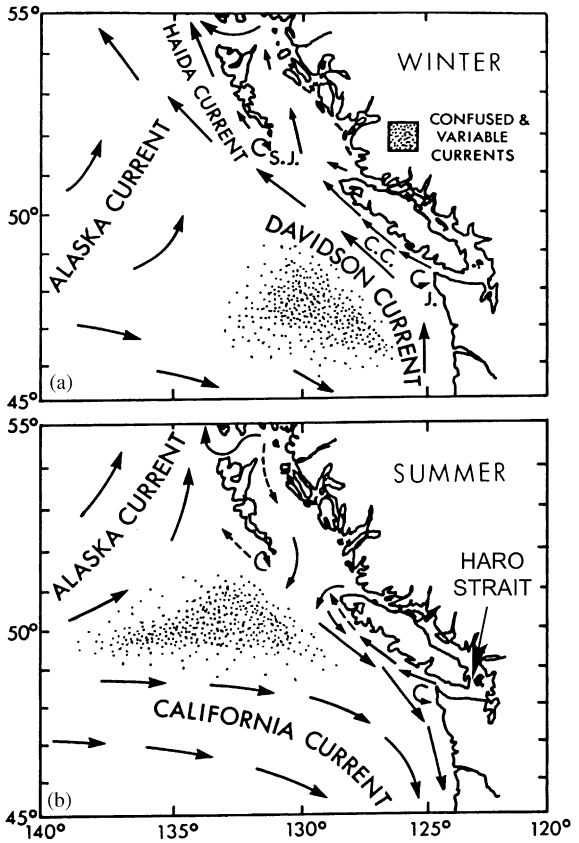


Fig. 2. The surface circulation patterns off the British Columbian coast during winter (a) and summer (b). Here the VICC is labelled as 'C.C.'. This figure has been reprinted from Thomson et al. (1989) with the permission of R. Thomson.

Coriolis force to create a northward flow that hugs the coast. This current runs counter to the equatorward surface current that flows over the mid- and outer-shelf in the summer. The equatorward current is part of the classical upwelling circulation (Smith, 1994). The VICC is also an important source of nutrients (due to intense mixing in Haro Strait (Fig. 2), the source of this current) and supports significant PP in the area (Mackas et al., 1980; Crawford and Dewey, 1989). In contrast, Vancouver Island is relatively pristine and delivers little organic matter or inorganic nutrient to the study area.

We describe the inorganic carbon system for each physical regime: the VICC, the outer-shelf and the slope, during downwelling and after upwelling. Biological uptake of carbon relative to nitrogen is compared for each of these regimes. Finally, daily carbon and nitrogen budgets are constructed and, along with the dominance of large phytoplankton cells, are contrasted for each regime. The implications of these results to annual carbon budgets are discussed.

## 2. Materials and methods

Data were gathered as part of the Canadian Global Ocean Ecosystem Dynamics program (GLOBEC) during July 1998 from the *CSS John P. Tully* along transects A (July 15), C (July 18), D (July 19) and G (July 23) (Fig. 1). Profiles of total dissolved inorganic carbon (DIC), total alkalinity (TA), nitrate ($NO_3^-$) and chlorophyll-*a* (chl*a*) were collected at each station (except DIC and TA were not sampled at G3 and G7, and $NO_3^-$ and chl*a* were not sampled at A9). Conductivity, temperature, depth (CTD) (Seabird Model SBE 911+ CTD) casts were made concurrently at each station and $\sigma_T$ calculated from temperature (T) and salinity (S) using the equations of Millero and Poisson (1981). At C4, C9, G3 and G7 total and size-fractionated primary production (PP), particulate organic carbon (POC) and particulate organic nitrogen (PON) were measured. Depths for these measurements were chosen by light levels (100%, 50%, 30%, 10%, 3% and 1% of surface photosynthetically available radiation (PAR) for PP and 100%, 50%, 10% and 1% for POC and PON) that were determined by a Biospherical QSP-200 L4S 4495 PAR sensor (Harris, 2001). A total of 114 DIC and 49 TA samples were collected. Additional samples for $NO_3^-$, chl*a*, as well as ammonium, phosphate, silicic acid and samples for nitrogen uptake experiments were also gathered in the study area as part of the GLOBEC project (Harris, 2001; unpublished data).

### 2.1. Analysis of seawater

Seawater samples were collected in acid-cleaned 10-l PVC Niskin bottles equipped with Teflon coated springs and fittings and silicon tubing mounted on an instrumented rosette sampler.

DIC and TA samples were drawn from the bottles according to the collection methods of Dickson and Goyet (1994), and samples for $NO_3^-$, chl*a*, PP (triplicate) and POC–PON (duplicate) were drawn according to the methods of Parsons et al. (1984). DIC was then determined coulometrically (Johnson et al., 1985, 1987) and TA samples were titrated (Millero et al., 1993). $NO_3^-$ plus nitrite ($NO_2^-$) was measured on filtered (with combusted GFF 0.7 μm filters) samples with a Technicon™ Autoanalyzer II (Wood et al., 1967) and the total reported as $NO_3^-$ (since $NO_2^-$ represents $\leqslant 5\%$ of the total $NO_3^- + NO_2^-$). Chl*a* (0.7 μm filter) was determined by in vitro fluorometry (Parsons et al., 1984). Rates of primary production were estimated using the $^{14}C$ technique (Parsons et al., 1984). PP samples (70 ml) were inoculated with 0.37 MBq of $^{14}C$ and incubated for 6 h under in situ light conditions as simulated with neutral density screening, and size fractionation (0.7 and 5.0 μm) was done by gravity filtration at the end of the incubation (Harris, 2001). (To convert to daily PP, data were multiplied by the total daily light (measured on the cruise) divided by the light during the measurement interval (Harris, 2001). POC and PON samples were filtered (0.7 μm), dried and analyzed with a Carlo Erba Elemental Analyzer (Verardo et al., 1990). This analysis measures all particulate carbon (C) and nitrogen (N) present; thus it is assumed any inorganic forms of N and C are negligible relative to the organic forms.

### 2.2. Data analysis and calculations

The partial pressure of carbon dioxide ($pCO_2$) was calculated from TA and DIC measurements using the relations of Dickson and Goyet (1994). Gas flux ($G$) was then estimated from the uppermost $pCO_2$ ($pCO_{2w}$) at each station (usually $\leqslant 2$ m) using the standard equation:

$$G = \alpha k(pCO_{2a} - pCO_{2w}), \tag{1}$$

where $\alpha$ is the solubility of $CO_2$ (estimated from T and S (Dickson and Goyet, 1994)), $k$ is the piston velocity and $pCO_{2a}$ is the atmospheric $pCO_2$ (380 ppm). We used averaged wind data (over a 1 d interval) from Meteorological Buoy 46206 (Fig. 1) in accordance with the Wanninkhof (1992) $k$-relationship derived from long-term averaged wind speed to estimate $k$. Since our time interval is short (1 d), we note that use of Wanninkhof's instantaneous relationship (rather than long-term) yields a 20% lower estimation of $k$ (and thus gas flux) relative to our estimate.

We constructed instantaneous budgets for DIC and $NO_3^-$ for spatial scales $\leqslant 10$ km (approximately the Rossby radius; i.e. the expected cross-shore correlation length for physical properties) on transects C and G over the mid-shelf and slope where PP was measured. The conservation equation for a scalar was used assuming that alongshore gradients were small enough (over an order of magnitude less than cross-shore gradients) to neglect. For DIC in the upper layer,

$$\frac{\partial \mathrm{DIC_u}}{\partial t} = -u_\mathrm{E}\frac{\partial \mathrm{DIC_u}}{\partial x} - \frac{\mathrm{PP}}{h_\mathrm{u}} + \frac{M}{h_\mathrm{u}}(\mathrm{DIC}_{l1} - \mathrm{DIC_u}) + \frac{G}{h_\mathrm{u}} + r_\mathrm{d}\mathrm{DOC_u}. \tag{2}$$

Terms on the right-hand side of the equation represent advection (Ekman transport), primary production, vertical mixing and entrainment, gas flux, and remineralization of DOC, respectively (Fig. 3): $t$ is time, $x$ is the horizontal cross-shelf dimension increasing offshore, $u_\mathrm{E}$ is the Ekman velocity in the $x$-direction, subscript u denotes the upper mixed layer and $h_\mathrm{u}$ is the mixed layer depth. $\mathrm{DIC_u}$ is the average DIC concentration in the mixed layer, $\mathrm{DIC}_{l1}$ is the concentration 1 m below $h_\mathrm{u}$ and $M$ is the vertical transport coefficient, including mixing and entrainment (units of velocity). DOC is the average concentration of the semi-labile dissolved organic carbon in the upper mixed layer and $r_\mathrm{d}$ is its remineralization rate. These terms were estimated from data (described below) and the time rate of change (left-hand side of the equation) was calculated from their sum. The $NO_3^-$ equation is identical except that there is no gas flux.

The velocity $u_\mathrm{E}$ within the mixed layer was estimated from the standard equation for Ekman transport (e.g. Gargett, 1991). (This equation relates wind stress, latitude and fluid density with

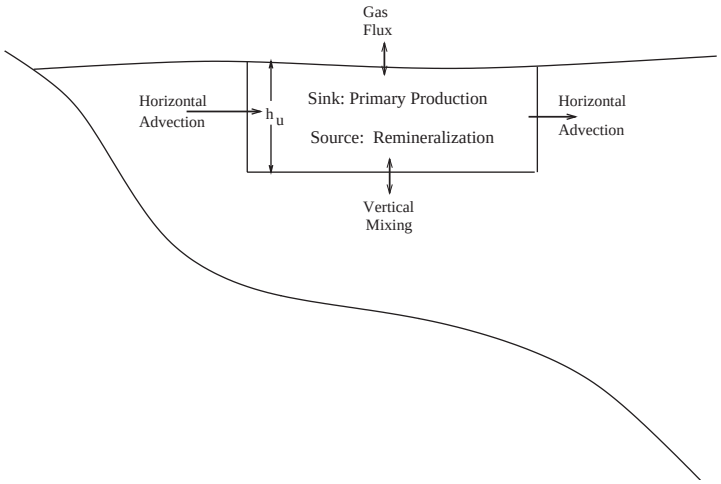


Fig. 3. The fluxes in the DIC budget (Eq. (2)). The time rate of change within the box (depth, $h_u$) is a sum of the physical transfer (shown by arrows) and the source and sink terms within the box. Fluxes in the $NO_3^-$ budget are identical except there is no gas flux.

$u_E$.) Wind stress was calculated from wind speed (Large and Pond, 1981) and it was assumed that half the total Ekman transport occurred within the mixed layer (Lentz, 1992). Horizontal gradients were estimated using the upwind differencing method (Press et al., 1992). (This method assumes that horizontal gradients at a point can best be approximated by those that are moving toward the point, i.e. coming from 'upstream'.) Vertical flux is difficult to approximate using estimates of vertical eddy diffusivity or equivalently diffusive velocity (i.e. the eddy diffusivity normalized by the thickness of the pycnocline) (e.g. Archer, 1995). Instead, we assume that the 2 m of fluid below the mixed layer is mixed or entrained into the upper layer each day (matched by mixing or detrainment of the same volume from the upper layer into the lower), based on daily fluctuations of mixed layer depths in the area (Thomson and Fine, 2003). Thus $M$ is 2 m $d^{-1}$.

Unfortunately, the DOC samples that we collected were contaminated so the remineralization term was based on DOC data from the Oregon upwelling region (Hill, 1999) assuming that the semi-labile fraction of the DOC is about 0.3 of the total (Carlson and Ducklow, 1995; Carlson et al., 1994) and the rate $r_d$ is 0.005 $d^{-1}$, based on a numerical modelling study of the area (Ianson and Allen, 2002). We estimate the remineralized flux of DON using the same data (again assuming that one-third of the bulk is semi-labile) and $r_d$ of 0.0065 $d^{-1}$ (Ianson and Allen, 2002).

## 3. Results and discussion

### 3.1. Physical data

We used temperature–salinity ($T$–$S$) data to identify water masses (VICC, inner-shelf, outer-shelf and slope) and wind and current data to show the physical state (upwelling, downwelling or relaxation) of each transect at the time of sampling. Upwelling occurs when winds (and alongshore current flow) are equatorward. We term intervals where the wind reverses direction (currents weaken and may reverse direction in the extreme case) as downwelling. Relaxation periods refer to the times between events (up- and downwelling or consecutive events of the same type).

Our data were collected during a weak ENSO year (indicated by wind anomalies and local sea-surface temperatures) following a strong ENSO year (1997) (http://www.pac.dfo-mpo.gc.ca/sci/psarc/OSRs/Ocean99fnl.PDF). Nevertheless, $T$–$S$ characteristics are in good agreement with the patterns described by Freeland et al. (1984). The

VICC is shown clearly as colder (as much as 4°C colder above 50 m, A1 Fig. 4), fresher (0.5 in salinity compared with the slope above 50 m) water over the inner-shelf along transects A, C (Fig. 4a) and D. Further north (Line G) there was little evidence of the VICC. If it was present, significant mixing had occurred between it and the equatorward current (Fig. 4b, $T$–$S$ are similar over the entire shelf and are warmer and fresher than the VICC (shown by A1)). Along Line C there was a fresh estuarine wedge originating from Barkley Sound outflow shoreward of C2 (note the depths of the $T$–$S$ point ($T = 9.81$, $S = 31.87$) decrease moving offshore, Fig. 4a), and VICC water was found beneath this wedge from C1 seaward to the shelf-break, including C4 and influencing C7, further offshore than expected. This wedge was likely enhanced by a strong storm with heavy rainfall several days prior to sampling the C line. A similar offshore deflection of the VICC due to an outflow event from Barkley Sound was observed during July 1984 (Hickey et al., 1991). Surface $T$–$S$ data from stations over the slope were all saltier (as much as 1) and slightly warmer ($<1$°C) than those from the outer-shelf, but at depths below roughly 40–50 m $T$–$S$ were similar at all stations. Isopycnals do not appear to tilt up or down moving onshore. Thus there is little evidence of upwelling (or downwelling) in the $T$–$S$ data (note the depths of the $T$–$S$ point ($T = 8.85$, $S = 32.7$) Fig. 4) (although there is a bulge in salinity at G4 25–29 m below the surface, indicated by the 'X' in Fig. 4b, that may have been caused by upwelling). However, upwelling occurred only towards the end of the study.

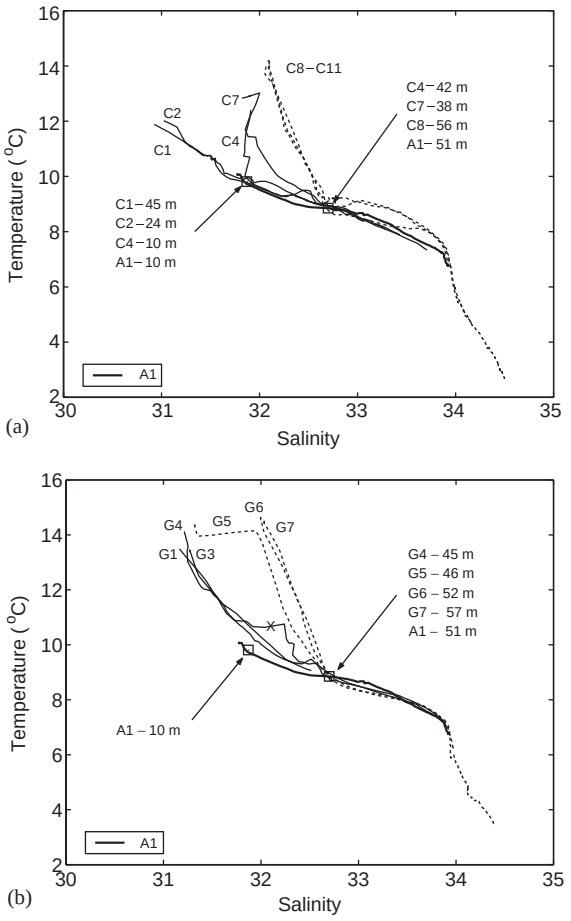


Fig. 4. $T$–$S$ curves for the C (a) and G (b) transects (over the shelf, solid line —; over the slope, dashed line, - -). The VICC is indicated by the $T$–$S$ from A1 (thick solid line). The depths for all stations passing through two $T$–$S$ points, ($T = 9.81$, $S = 31.87$) and ($T = 8.85$, $S = 32.7$), marked by open squares, are indicated for comparison. The X (in b) marks a bulge in G4 salinity at 26–29 m. Note that below ~50 m the water masses have overlapping $T$–$S$ at all locations. The upper left portion of the plot contains the surface water from each station. In (a) the surface water of stations C1 and C2 is part of the fresh estuarine wedge originating from Barkley Sound. The surface water of stations C8–C11 (in a) and G5–G7 (in b) is typical for the slope, while G1, G3, and G4 (in b) are only slightly fresher.

Winds along the BC coast have a strong alongshore principal axis and are spatially coherent over lengthscales of 100s of km (Faucher et al., 1999; Hsieh et al., 1995). Data from a meteorological buoy (MB, Fig. 1) located in the center of our study area (as well as the Bakun upwelling index) show that upwelling was reasonably strong beginning in May and continuing through early-mid July when our study began. Between July 11 and 18 (peaking in a rare summer storm on July 14) winds were downwelling favorable (poleward) (Fig. 5) and the equatorward surface current reversed direction (R. Thomson, pers. com.). Much of our data were collected during and at the end of this period. Line A was sampled right after the storm (July 15) and Line C just after the transition back to normal, but weak, upwelling favorable winds (July 18). On July 21 local winds increased and an upwelling event occurred (Fig. 5;

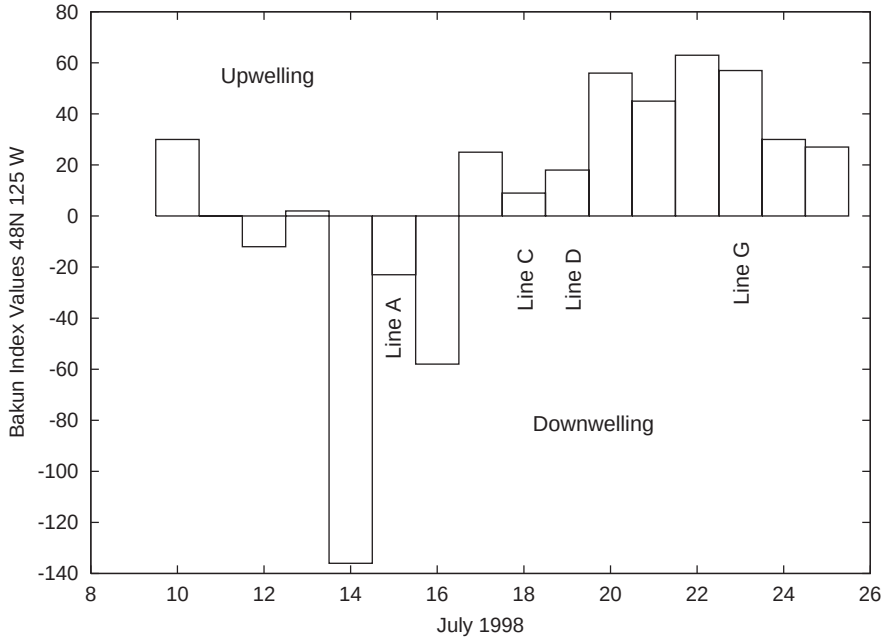


Fig. 5. The Bakun upwelling index for 48°N 125°W (just south of Line A) (from http://www.pfeg.noaa.gov/products/PFEL/modelled/indices/upwelling/NA/) during our study period. Indices have units of $m^3\ s^{-1}$(100 m coastline)$^{-1}$. Positive numbers indicate upwelling (offshore transport) and negative downwelling. These data were provided courtesy of the Pacific Fisheries Environmental Laboratory.

R. Thomson, pers. com.). (Note that the Bakun upwelling index shows the increase one day prior, July 20 (Fig. 5).) Data from the D line were collected before this event (July 19) and from the G line 3 days later (July 23). Thus, we consider transects A and C to be during summer downwelling, D during a relaxation period, and G after an upwelling event.

### 3.2. Inorganic carbon data

There are three distinctive features in the inorganic carbon system in the coastal upwelling region west of Vancouver Island. These features are shown in vertical DIC profiles normalized by salinity (to remove affects of fresh water runoff, precipitation and evaporation) (Fig. 6). We normalized to a salinity representative of our data ($S = 32$) to introduce as little bias (from assuming that the DIC-S dilution line passes through the origin) as possible. Thus, normalized data = measured data × 32/measured salinity.

First, the VICC has high surface values at A1 and C2, which are diluted (and biologically drawn down) by the time the current reaches D1. Elsewhere, biological drawdown of DIC is evident in the surface waters. This drawdown is strongest over the outer shelf relative to the slope (where sampled). Third, the deeper (> 50 m depth) water over the outer shelf is always higher in DIC than over the slope at the same depth.

To explain the higher shelf DIC, we first discount upwelling in these data and then propose an alternate mechanism. The bulge around 30 m at G4 (Fig. 6) may be the bottom portion of the Ekman layer (i.e. below the surface mixed layer) resulting from recent upwelling inshore of G4. (This bulge is also seen in salinity, Fig. 4b marked by an 'X'.) On the other lines, however, there was no upwelling (see Section 3.1) so the elevated DIC is likely due to remineralization of organic matter delivered from the productive surface waters over the shelf. This organic matter falls into a significantly smaller (depth-shelf(depth-slope)$^{-1}$)

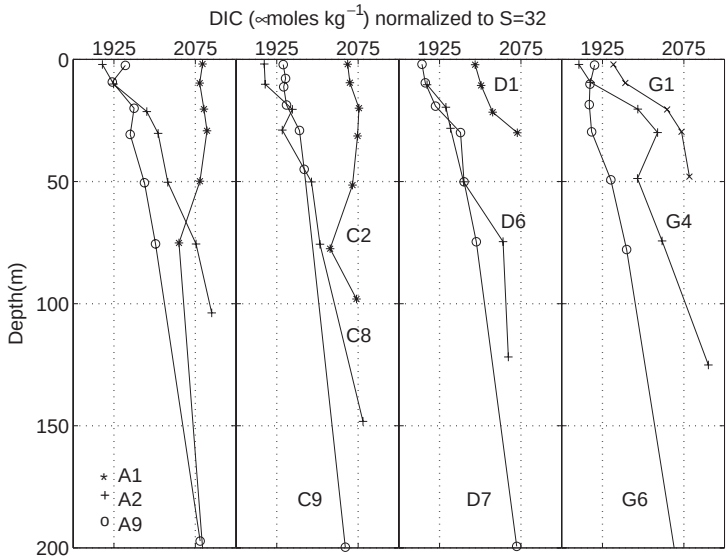


Fig. 6. DIC profiles are shown from Line A, C, D, and G, in panels left to right, for outer slope stations (o), outer shelf stations (+), inner shelf stations north of the VICC (x) and in the VICC (*). All data are normalized to a salinity of 32. Units are converted from μM to μmoles kg$^{-1}$ using the calculated density of seawater.

volume of lower layer water because the shelf is shallower. Thus the remineralized carbon is more concentrated, making for higher total carbon inventories (per volume) over the shelf relative to the slope. (The carbon inventory is the sum of all forms of carbon in the water column (normalized by volume); however the inorganic form is by far the dominant.) To maintain these high inventories there must be a balance between the delivery of organic material and physical processes that dilute them (mixing and advection). A modelling study of annual cycles in the area (Ianson and Allen, 2002) shows that this balance can be maintained in a positive feedback loop. Upwelling circulation keeps DIC (and $NO_3^-$) over the shelf (as well as introducing potentially high concentrations) by advecting it into the surface where it can be converted into POC via PP. A fraction of the PP sinks (going in the opposite direction of the advective circulation), where most is remineralized and can be advected (or mixed) back into the surface. When (exported) PP is higher, the enrichment in DIC (and $NO_3^-$) is (are) greater. Similarly, higher $NO_3^-$ (or limiting nutrient) concentrations in the lower layer make for increased PP.

The variation of DIC and TA with salinity has been described by others using linear regressions (e.g. Kempe and Pegler, 1991; Takahashi et al., 1991). If these relationships are truly linear then they suggest that both DIC and TA concentrations are controlled by dilution (evaporation, precipitation and run-off). Biological fluxes (uptake and remineralization of DIC and in the case of TA, $CaCO_3$ formation) occurring at different depths (and thus salinities) as well as surface DIC exchange (which is $T$ dependent) cause non-linear variations with salinity (e.g. Millero et al., 1998). In addition, mixing of more than one water mass that has differing biological activity (or that have different non-zero DIC concentrations in their freshwater ($S = 0$) source) can cause non-linearities. We have calculated linear regressions (Model I, using salinity as an independent variable) from our data over specific depth ranges to discuss deviations from linearity and to compare with the regressions of others (Fig. 7).

As expected given the normalized vertical profiles (Fig. 6), our DIC data are not linear with salinity over all depths (Fig. 7a). Thus, we present a regression for all DIC data below the mixed

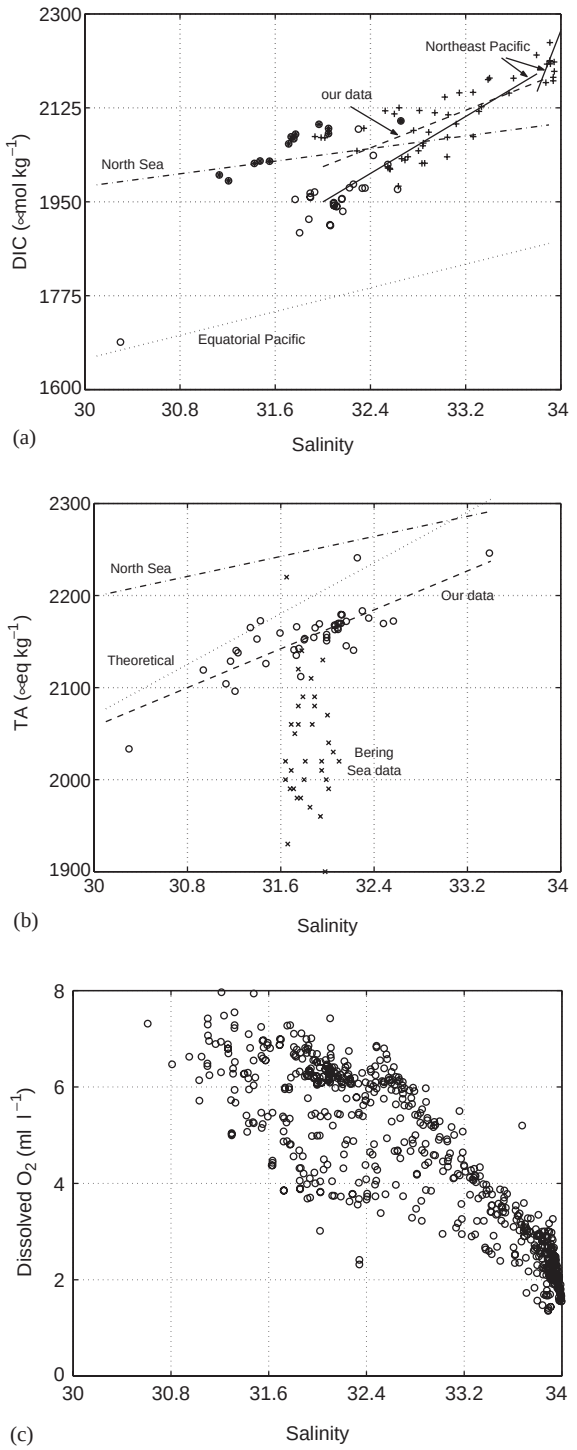


layer. Most surface DIC samples fall below the regression line due to biological drawdown; those in the VICC are all above the line because the VICC is rich in DIC. Our DIC measurements compare well with those made offshore of the study area in the Northeast Pacific (from station P04 (similar to our outermost slope stations, Fig. 1) to P26 (50°N, 145°W)) during all seasons from 1986 to 1993. These data appear linear in two distinct depth regions; the first for mid-depths, 40–180 m (excluding surface samples where biological and gas fluxes are likely to be important) and the second below that (at higher salinity) for depths 180–400 m. Data from the latter depth range are all from P04. We assume that there is more DIC (per salinity) below 180 m due to remineralization of particulate organic matter of both local and remote origin. The regression from our shelf and slope data is slightly higher than the mid-depth offshore data due to higher DIC values (per salinity) over the shelf. Our deepest samples (too few to make a separate regression) also appear to follow the steeper regression from P04, although they are from the shallow end of the depth range.

Oxygen data collected concurrently during our study (courtesy R. Thomson and D. Yelland), also

Fig. 7. (a) Upper layer (o) and lower layer (+) DIC data are plotted against salinity. The upper layer was defined as 20 m and above for stations over the shelf and 30 m and above further offshore. DIC samples from within the VICC (all upper layer) are also marked with a *. A linear regression (– dashed lines) of the lower layer DIC data is: DIC = 87.6$S$–787 μmole kg$^{-1}$ ($r^2 = 0.75$). DIC from Line P (mainly P04) in the Northeast Pacific are shown by two linear regressions (– solid lines): DIC = 133$S$–2293 ($r^2 = 0.84$, from 293 data) for depths 40–180 m ($S < 33.8$) and DIC = 568$S$–17043 ($r^2 = 0.84$, from 95 data) for depths 180–400 m ($S < 33.8$). A DIC regression from the North Sea ( – · dash-dot lines) (Kempe and Pegler, 1991) and an open ocean regression (·· dotted line) from data in the equatorial Pacific (Takahashi et al., 1991) are shown. (b) TA data from all depths (o) are plotted against salinity. TA data from the Bering Sea (Codispoti et al., 1986) where $CaCO_3$ production occurred are also shown (x). A linear regression (– dashed lines) of our TA data is: TA = 52.85$S$ + 472 μeq kg$^{-1}$ ($r^2 = 0.80$). TA regressions from the North Sea data ( – · dash-dot lines) (Kempe and Pegler, 1991) and from theory (·· dotted line) (Skirrow, 1975) are shown. (c) Oxygen data collected concurrently plotted against salinity (same range as above). Note that more oxygen samples were made during this study than DIC or TA.

plotted against salinity, (Fig. 7c) confirm this remineralization hypothesis. Similarly in the depth range 180–400 m ($\sim 33.7 < S > 34$) oxygen values drop more rapidly with salinity indicating increased consumption due to remineralization of organic matter.

To put our DIC–$S$ data in context with other studies, we show regressions of coastal summer DIC data in the North Sea (Kempe and Pegler, 1991) as well as an open ocean regression from the equatorial Pacific (Takahashi et al., 1991). Some surface data have been reported for fresher water (salinity 23–27) inshore of Vancouver Island (Johnson et al., 1979). These DIC data fall between predictions from our regression and the North Sea regression, indicating that inshore surface waters are not the source of the elevated DIC in the VICC and suggesting that local fresh water sources do not supply excess DIC. The coastal data sets have higher DIC per salinity than the equatorial open ocean data, particularly above 32–33, the range in which most coastal data occur. This disparity is expected as water temperatures in the equatorial Pacific are higher thereby reducing the carbon capacity. We suggest that carbon inventories may be higher in coastal waters than in the open ocean because remineralization of organic carbon from high coastal primary production is concentrated in a smaller water volume. This mechanism provides positive feedback (discussed above), as high inventories of inorganic nutrients make for larger vertical fluxes of nutrients into the euphotic zone leading to higher primary production (Ianson and Allen, 2002).

Unlike the North Sea DIC regression, our regression has a negative DIC intercept ($-787$ μmole kg$^{-1}$). It is likely that particulate flux of organic matter to deeper waters during the summer makes for elevated deep water DIC (where salinity is higher) via remineralization throughout the study area (seen most clearly over the outer shelf in Fig. 6). Elevated values of DIC at higher salinities would tend to increase the slope of a DIC–$S$ regression and could give rise to a negative intercept. The positive DIC intercept in the North Sea data would be expected to represent DIC concentrations in terrigenous fresh water sources there.

Our TA data appear linear in salinity (Fig. 7b) over all measured depths showing that precipitation and evaporation exerted the major control over TA during our study. The regression of our TA data is close to the theoretical regression predicted by Skirrow (1975), but it has a positive intercept (470 μeq kg$^{-1}$) likely due to concentrations of dissolved salts in the runoff from Vancouver Island. Riverine input can have appreciable TA (e.g., Milliman, 1993). (Note that if biological calcium carbonate ($CaCO_3$) production occurred in the higher salinity samples, but not the lower, a positive intercept could also result.) $CaCO_3$ formation was not an influence during our study although a coccolithophorid bloom occurred during 1997 (unpublished data). Data from the Bering Sea (Codispoti et al., 1986) fall well below our regression, and are not linear in $S$, due to $CaCO_3$ production by coccolithophores. The North Sea data regression (Kempe and Pegler, 1991) is much higher possibly due to a higher terrestrial input of $CaCO_3$ into the North Sea.

The range in $pCO_2$ of surface waters was extreme; from 117 ppm (at G4 after upwelling) to 1734 ppm (A1 near the source of the VICC) (Table 1). All estimates of $pCO_2$ within the VICC are exceptionally high (mostly > 1000 ppm), with the exception of the surface value at C1 which is significantly fresher ($S < 31$) and has low DIC; presumably this sample contains some fresh water outflow from Barkley Sound with VICC water underneath. Given the high $pCO_2$, the predicted gas outflux from the VICC is high, particularly at A1 and C2. Outside the VICC, gas flux changes sign and is always into the ocean (with the exception of A9). The greatest observed influx occurs over the outer shelf where biological drawdown of DIC is strongest. This influx is highest after upwelling (sampled at G4). Over the slope, $pCO_2$ is much closer to equilibrium (e.g. C9, C10 and C11).

### 3.3. Organic carbon data

PP, POC and chl*a* (Table 2) were determined from samples along transects C and G at shelf stations (C4, G3) and slope stations (C9, G7). When sea water is filtered to make these

Table 1
$pCO_2$ for all depths where both TA and DIC were measured on transects A, D and G (a) and C (b) (July, 1998)

| | $pCO_2$ (ppm) | | | | | | Gas flux |
|---|---|---|---|---|---|---|---|
| | 2 m | 8 m | 10 m | 20 m | 45 m | 100 m | (mmol C $m^{-2}$ $d^{-1}$) |
| (a) Transects A, D and G | | | | | | | |
| A1 | 1734 | | 1384 | 2251 | | | −44 |
| A2 | 244 | | 292 | | | | 3.3 |
| A9 | 451 | | | 533 | | | −3.2 |
| D1 | 406 | | 441 | 556 | | | −1.8 |
| D6 | | | 252 | 364 | | | 3.0 |
| D7 | 242 | | 241 | | | | 3.3 |
| G1 | 286 | | 289 | 925 | | | 2.0 |
| G4 | 117 | | 207 | 419 | | | 5.4 |
| G6 | 296 | | 280 | 264 | | | 1.7 |
| (b) Transect C | | | | | | | |
| C01 | 112 | | 1030 | 690 | | | 7.6 |
| C02 | 1080 | | 1190 | 1280 | | | −24 |
| C04 | | | 380 | | | | −1.0 |
| C07 | | | 410 | 1210 | | 1740 | −1.9 |
| C08 | 260 | | 260 | 390 | | | 2.7 |
| C09 | | 350 | 350 | 270 | 540 | | 0.1 |
| C10 | | | 310 | | | | 1.2 |
| C11 | | | 330 | 330 | | | 0.6 |

Air–sea gas flux is negative for gas evasion from the surface ocean to the atmosphere and positive for gas invasion. We estimate the uncertainty in the $pCO_2$ calculation as 4% (based on the results of Wanninkhof et al. (1999) in the temperature range 5–15°C).

Table 2
Particulate organic carbon (POC), chlorophyll*a* (chl*a*), primary production (PP), % of the total PP in the size class > 5.0 μm (mainly diatoms), C:chl*a*, POC:PON and $NO_3^-$ averaged over the euphotic zone (EZ) (6 depths for PP and 4 depths for POC) (a) and at discrete depths (*d*) (b) at stations C4, C9, G3 and G7 (July 1998)

| Stn | EZ (m) | POC (μmol $m^{-2}$) | chl*a* (mg $m^{-2}$) | PP (mgC $m^{-2}$ $h^{-1}$) | % PP > 5.0 μm | C:chl*a* (g:g) | POC:PON (mol:mol) | $\overline{NO_3^-}$ (μM) |
|---|---|---|---|---|---|---|---|---|
| (a) Integrated | | | | | | | | |
| C4 | 42 | 706.9 | 107.3 | 969.7 | 87 | 79 | 5.6 | 12.4 |
| C9 | 45 | 490.7 | 66.9 | 243.6 | 62 | 88 | 6.4 | 1.2 |
| G3 | 30 | 1134.2 | 242.3 | 649.5 | 84 | 56 | 5.9 | 8.2 |
| G7 | 44 | 480.3 | 32.2 | 334.6 | 70 | 180 | 6.0 | 0.0 |
| Stn | *d* (m) | POC (μM) | chl*a* (mg $m^{-3}$) | PP (mgC $m^{-3}$ $h^{-1}$) | % PP > 5.0 μm | C:chl*a* (g:g) | POC:PON (mol:mol) | $NO_3^-$ (μM) |
| (b) Discrete depths | | | | | | | | |
| C4 | 0 | 46.31 | 9.0 | 154.1 | 94 | 62 | 5.5 | 4.4 |
| C9 | 19 | 13.17 | 1.2 | 5.5 | 51 | 130 | 6.3 | 0.0 |
| C9 | 30 | | 2.8 | 5.9 | 85 | | | 0.3 |
| G3 | 0 | 53.81 | 14.2 | 45.8 | 93 | 45 | 5.9 | 0.9 |
| G7 | 6 | | 0.4 | 42.79 | 84 | | | 0.0 |
| G7 | 44 | 16.28 | 3.0 | 1.0 | 46 | 65 | 5.9 | 0.0 |

Discrete depths were chosen where PP and chl*a* were high (relative to other depths) for comparison with averaged values (see text). At C9 (30 m) and G7 (6 m), POC and PON data were not available at these depths so another depth where all data were available was also included (19 m for C9 and 44 m for G7).

measurements, non-living detritus and dormant cells are collected as well as living phytoplankton cells. We present values integrated over the euphotic zone and representative of all the above forms of POC (Table 2a). In addition, the fraction of the total PP from the > 5.0 μm size class (representative of diatoms), C:chl*a*, POC:PON ratios and average $NO_3^-$ concentration ($\overline{NO_3^-}$) are presented. To contrast with these data (particularly with the ratios) we include data from discrete depths (Table 2b) where PP and chl*a* were high relative to other depths to represent samples with a larger fraction of viable phytoplankton.

PP at C4 was even higher than expected given the large supply of nutrients from the VICC (particularly at the surface, Table 2b). (Total nitrogen (both nitrate and ammonium, but less urea) uptake was also high (3 mg N $m^{-3}$ $h^{-1}$) in the surface at C4 relative to other stations (unpublished data).) After upwelling PP was high over the shelf (G3) (although the largest upwelling response was centered at G4, discussed below). Over the slope (C9, G7) PP was lower. Large diatom cells dominated at all stations (Harris, 2001), but particularly where PP was higher due to the supply of new inorganic nutrients (*sensu* Hutchings et al., 1994). POC:PON was relatively constant (range 5.6–6.4) between stations and close to the Redfield ratio (Redfield et al., 1963). Also this ratio was constant regardless of the fraction of the particulate organic matter that was living (compare values from the discrete depths having a higher portion of viable phytoplankton with integrated values; i.e., Table 2a and b). Thus, there was no evidence of variable C:N incorporation by phytoplankton or of preferential remineralization of particulate carbon or nitrogen in the surface.

It is expected that non-living POC is low in chl*a* and our data are in agreement with this expectation. C:chl*a* varied considerably between integrated and discrete samples. The ratio was much lower (45–62) over the shelf at discrete depths (surface) in Table 2) that had a higher fraction of viable phytoplankton relative to the integrated data. Over the slope (C9 and G7), where this fraction was estimated to be highest, C:chl*a* could not be calculated because POC data were not available. In the integrated samples C:chl*a* was always higher (than at discrete depths where PP and chl*a* were high) and had a larger range (56–180). At G3 (after upwelling), the ratio had the smallest range, presumably because more of the integrated POC was living. At G7, the integrated C:chl*a* was high, likely because $NO_3^-$ was recently (over a period of days) exhausted and a bloom had just crashed. Phytoplankton may also reduce their cellular chl*a* when nitrogen is limiting and light is plentiful (Laws and Bannister, 1980; Taylor et al., 1997) which could add to the observed increase in the C:chl*a* ratio particularly at G7 (note the high PP relative to low chl*a* at 6 m (Table 2b)).

### 3.4. Variations in inorganic carbon and nitrogen

We use chl*a*, $NO_3^-$ and DIC spatial patterns from line C and G to contrast summer downwelling with upwelling and the VICC (Fig. 8). The data have not been smoothed. Where $NO_3^-$ and DIC values do not increase with depth (instead there is a sign reversal in the vertical gradient; e.g., $NO_3^-$ at C10 is 4 μM higher at 100 m than at 125 m) the contours have small sharp changes.

The VICC can clearly be seen in high chl*a* values in the upper 20 m (Fig. 8a, upper panel) extending from C2 to C7. (Our T, S (Fig. 4) and $pCO_2$ (Table 1) data show the location of the VICC at the time of sampling.) The VICC is not expected to extend as far seaward as C7, although it has been previously observed to do so (Hickey et al., 1991). In addition to high chl*a*, the VICC has high $NO_3^-$ and high DIC (Fig. 8a, middle and lower panel, respectively). Seaward of the VICC (C8–C11) summer downwelling conditions showed low concentrations of chl*a* at all depths and of $NO_3^-$ above 100 m. DIC concentrations were moderate and depressed in the surface just beyond the VICC at C8 and C9. The most notable feature in the summer downwelling region was the low concentrations of inorganic nutrients (DIC and $NO_3^-$) below the euphotic zone due to the deepening of the nutricline.

Transect G showed a strong response to upwelling in chl*a* (with values roughly twice as high as in the VICC) centered on G4 and

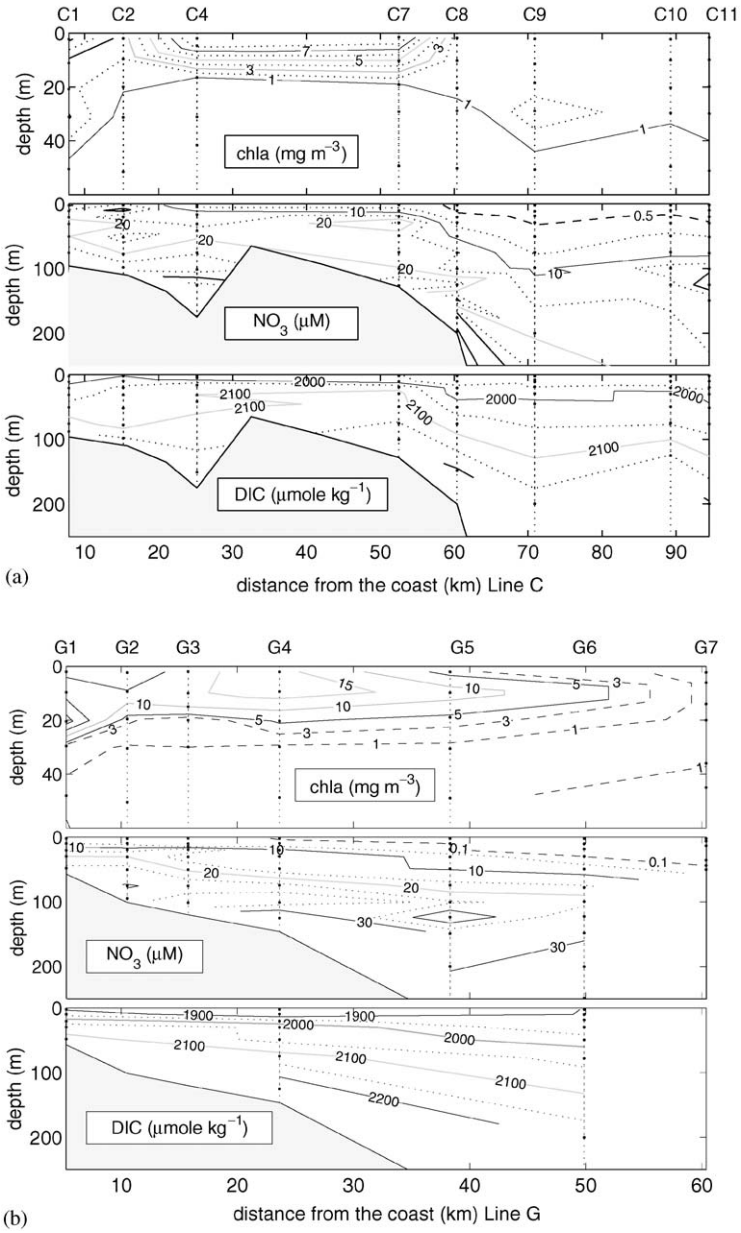


Fig. 8. Contours of chl*a*, $NO_3^-$ and DIC along line C (a) and line G (b). Note that the depth range is only 50 m for chl*a* (where data were gathered) compared to 250 m for $NO_3^-$ and DIC. Grey shading marks the bottom topography. Occasional sharp changes in contours reflect the data (that have not been smoothed) as discussed in the text.

extending seaward over the slope almost to G7 (Fig. 8b, upper panel). Surface (15–20 m over the shelf, 40–50 m over the slope) values of $NO_3^-$ were low (Fig. 8b, middle panel). Below 50–100 m, however, $NO_3^-$ concentrations were high. Here the contrast between upwelling (line G) and downwelling (C8–C11) is evident as the 20 μM contour was above 50–80 m after upwelling and between

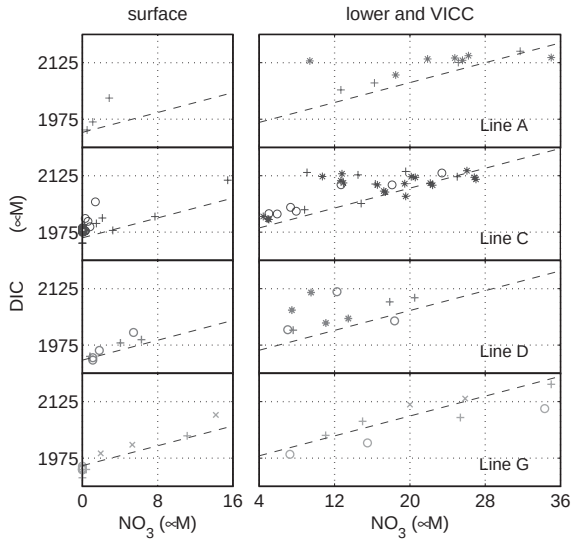


Fig. 9. DIC (μM) is plotted against $NO_3^-$ (μM) for surface values (left column) and sub-surface values (right column) to compare ΔDIC : ΔDIN for stations on transects A, C, D and G. All values (DIC and $NO_3^{-1}$) are normalized to a salinity of 32. All values (surface and sub-surface) within the VICC (*) are included with the sub-surface data. Outer shelf stations (+), inner shelf stations that are not part of the VICC (x) and slope—offshore stations (o) are separated into surface and sub-surface stations based on mixed layer depths (<20 m over the shelf and <30 m for the outer stations). The theoretical Redfield slope (C:N = 6.6) (- - dashed line) is plotted for each transect with different DIC intercepts (1940, 1960, 1935 and 1955 μM for lines A, C, D and G, respectively) to correspond with the data.

150 and 250 m after downwelling. Contours were also smoother and more horizontal after upwelling. Biological drawdown of DIC after upwelling (and the absence of the VICC) caused much lower surface values (a depression of $>150$ μmol $kg^{-1}$ relative to line C) coincident with the high chl*a* patch (Fig. 8b, lower panel). DIC increased rapidly below the surface, however, and like $NO_3^-$, DIC concentrations are higher at shallower depths after upwelling than after downwelling.

DIC data were plotted against $NO_3^-$ (Fig. 9) to estimate C:N ratios of biological uptake and remineralization in our data. All data (DIC and $NO_3^{-1}$) were normalized by salinity to account for effects of freshwater runoff, precipitation and evaporation. We chose to normalize to a salinity of 32, the average value for surface samples in which $NO_3^-$ was undetectable. To remove advective effects (caused by differing DIC:$NO_3^{-1}$ ratios in source waters), data from each line were plotted separately. Because transects were sampled on different days and during different physical states, these effects were large. (Data are widely scattered when surface data are plotted together.)

The slope ($\Delta DIC : \Delta NO_3$) represents a combination of biological uptake and remineralization of organic matter. The effects of air–sea $CO_2$ exchange on the slope are expected to be small but would serve to decrease the measured $\Delta DIC : \Delta NO_3$. By separating the data into surface (left column) and sub-surface (right column) plots we hope to separate biological uptake and remineralization, respectively. The theoretical Redfield C:N ratio (6.6) for these processes is included in each plot (dashed line) for comparison with our data. We do not have sufficient samples to make statistical regressions on our data.

On lines A, C and D (Fig. 9 upper, second and third panel, left column) during downwelling and relaxation periods, biological uptake appears to exceed the Redfield ratio. Note that the apparent trend in the data is steeper than the Redfield slope. The largest measured $\Delta DIC : \Delta NO_3$ occurs during downwelling (Lines A and C) when surface $NO_3^-$ was likely limiting (and for a longer period). After upwelling (Line G, Fig. 9 lower panel), when a large quantity of $NO_3^-$ has been recently supplied, $\Delta DIC : \Delta NO_3$ is close to the Redfield ratio. We could have also plotted lines with slopes of the measured POC:PON ratio (rather than the Redfield ratio) on transects C and G. However, the measured ratios are lower than 6.6, so this would only serve to decrease the slope making the excess carbon uptake larger.

Others have observed excess uptake of DIC relative to $NO_3^-$ in the field (Codispoti et al., 1986; Sambrotto et al., 1993) and in the lab (Goldman et al., 1992; Richardson and Cullen, 1995). Evidently, carbon is still processed by phytoplankton in the absence of nitrogen in response to light, although in our study it was not incorporated into the particulate organic matter as the surface POC:PON ratio remained constant (Table 2). Richardson and Cullen (1995) did observe an increase in cellular POC:PON under nitrogen

replete conditions. In addition the POC:PON ratio in the sedimenting flux below the euphotic zone (200 m) in the study area can be elevated (ranging from 6 to 10) (Peña et al., 1999). However, preferential remineralization of nitrogen (e.g. Toth and Lerman, 1977) could easily cause these changes in the sedimenting flux. We propose instead that phytoplankton may excrete the excess carbon uptake into the DOC pool. This mechanism could explain why measured DOC:DON ratios in the slope region of our study area (Wong et al., 1997) and in the Oregon upwelling region (Hill, 1999) are much higher (> 10) than the Redfield ratio.

Nutrients other than $NO_3^-$ may be limiting in upwelling regions (e.g. silicic acid (Dugdale et al., 1995), iron (Hutchins and Bruland, 1998)). However, during our study $NO_3^-$ was depleted before both phosphate and silicic acid and these nutrients were all highly correlated (Harris, 2001). Iron was not measured, although it is unlikely that it was limiting in our study area, close to a coastal region where terrigenous runoff is high.

Measured $\Delta DIC : \Delta NO_3^-$ below the surface mixed layer over the outer shelf and slope (Fig. 9 right side) are close to the Redfield ratio (again shown as a dashed line), suggesting that remineralization of organic matter (in situ or transported from elsewhere) occurs in a similar ratio. However, the VICC samples (marked by *) appear to have lower $\Delta DIC : \Delta NO_3$ (note that these data include surface values). DIC values are consistently high over a wide range of $NO_3^-$ concentrations. Denitrification in the source waters could cause the C:N disparity; however it is unlikely as Haro Strait is well oxygenated throughout the water column (R. Pawlowicz, pers. com.). Perhaps the VICC source waters were not influenced by recent remineralization of organic matter or remineralization is not occurring in accordance with the Redfield ratio.

### 3.5. DIC and $NO_3^-$ budgets

Inorganic carbon and nitrogen budgets for the VICC (C4) after downwelling (C9) and after upwelling on the outer shelf (G4) and slope (G6) show the importance of each term in Eq. (2) (Table 3). Physical transport and biological source and sink terms were estimated from data (see

Table 3
Terms in the daily DIC (a) and $NO_3^-$ (b) budgets for the upper mixed layer in the Vancouver Island Coastal Current (C4), after downwelling (C9) and after upwelling on the outer shelf (G4) and slope (G6) July 1998

| | C4 | C9 | G4 | G6 |
|---|---|---|---|---|
| (a) Daily DIC | | | | |
| Advection | $-11\pm5$ | $-1.0\pm0.2$ | $20\pm10$ | $-3\pm1$ |
| Biological uptake | $-8\pm2$ | $-1.2\pm0.6$ | $-7\pm3$[a] | $-1.4\pm0.6$[b] |
| Vertical flux | $4\pm2$ | $1.2\pm0.6$ | $5\pm3$ | $1.0\pm0.5$ |
| Gas flux | $-0.05\pm0.03$ | $0.003\pm0.001$ | $0.3\pm0.1$ | $0.04\pm0.01$ |
| Remineralization | $0.3\pm0.2$ | $0.3\pm0.2$ | $0.3\pm0.2$ | $0.3\pm0.2$ |
| $\frac{d}{dt}$ DIC | $-15\pm6$ | $-1\pm1$ | $20\pm10$ | $-3\pm1$ |
| (b) Daily $NO_3^-$ | | | | |
| Advection | $1.3\pm0.5$ | $0.04\pm0.01$ | $0.7\pm0.2$ | $0.0\pm0.1$ |
| Biological uptake | $-1\pm1$ | $-0.2\pm0.2$ | $-1\pm1$ | $-0.2\pm0.2$ |
| Vertical flux | $0.2\pm0.1$ | $0.04\pm0.02$ | $0.5\pm0.3$ | $0.10\pm0.05$ |
| Remineralization | $0.05\pm0.03$ | $0.05\pm0.03$ | $0.05\pm0.03$ | $0.05\pm0.03$ |
| $\frac{d}{dt}$ $NO_3^-$ | $1\pm1$ | $-0.1\pm0.2$ | $0\pm1$ | $-0.1\pm0.2$ |

All units are $\mu M\ d^{-1}$.

[a] Biological uptake of $NO_3^-$ was estimated from carbon uptake measurements assuming a C:N uptake of 6.6.

[b] Biological uptake at G4 and G6 were assumed to be the same as at G3 and G7, respectively.

Section 2) and the rate of change was calculated from their sum. Uncertainties in this estimation are large and come from four different sources: measurement error (how well a quantity is estimated from a water sample), representativeness or patchiness (how well that water sample represents the homogenized physical box), neglected processes (such as along-shore advection, discussed below) and unknown parameters or quantities ($r_d$, $M$ and DOM). Uncertainties are estimated based on the largest source of error for each flux. All measurement errors are negligible compared with the other sources of uncertainty. The largest uncertainty in horizontal advection, biological uptake and gas flux comes from 'representativeness or patchiness', estimated from variations in measurements within the respective transects (C and G). (The uncertainty in the Ekman transport calculation is (less than) 20% (Lentz, 1992).) Uncertainties in biological nitrogen uptake are large because it is estimated from carbon uptake using Redfield ratios, which are likely not followed (we estimate uncertainty as $\pm 100\%$). In the vertical flux term uncertainty in the value of $M$ (we estimate $\pm 50\%$) is much greater than other quantities in this term (e.g. the uncertainty in average upper layer DIC is $\sim 5\%$). The remineralization term is not based on measurements in our area (see Section 2) and is subject to large uncertainties. However, its magnitude is small relative to the other terms and so its uncertainty only affects the slope budgets.

Alongshore transport will be significant (say $\geqslant \frac{1}{10}$ cross-shore (Ekman) transport) to our budgets if horizontal gradients (of C or N) in the alongshore direction are large enough ($> 1/10$ cross-shore gradients) assuming that the alongshore currents are stronger (1–10 times) than in perpendicular direction (as expected). Alongshore data were collected on different days so these gradients are difficult to estimate. However, Lines C and D (Fig. 1) were sampled on consecutive days. These data yield alongshore gradients ($\partial/\partial y$) in DIC an order of magnitude less than cross-shore ($\partial \mathrm{DIC}/\partial y$) over both the shelf and slope. (Note that the sign of the alongshore gradient would make for a DIC source at C4 (assuming northward flow) and a sink at C9 (southward flow).) Gradients in $NO_3$ are not significant. Alongshore currents at this time (July 18–19) and when Line G was sampled (July 23) in the vicinity of C9 were not strong, of the same order as the cross-shore currents (R. Thomson, unpublished data). Thus, our estimates indicate that alongshore transport is unlikely to be significant to our budgets (of the same order as remineralization terms). It is important to note, however, that alongshore gradients in the vicinity of the VICC source (south) are likely larger.

After downwelling (C9), the system is near steady state with respect to both DIC and $NO_3^-$. Over the slope after upwelling (G6), $NO_3^-$ fluxes are close to steady state (Table 3b) but there is still a significant net cross-shore advective flux of DIC (Table 3a). The DIC budgets from both shelf stations are dominated by the cross-shore advective term due to strong cross-shore gradients. The VICC (C4) experiences a large net loss of DIC (although C4 may be close to steady state given the uncertainty) because concentrations there are much larger than they are in surrounding waters. This loss is likely compensated for by along-shore supply of DIC from the Juan de Fuca Strait (A1). In contrast, there is large net advective (cross-shore) import of DIC on the outer shelf after upwelling (G4) (again steady state is within the uncertainty) due to intense biological drawdown of DIC. Advective fluxes of nitrogen are important to the daily budgets over the outer shelf but they are of the same order as or less than other terms. Since $NO_3^-$ can be depleted rapidly by phytoplankton growth, surface concentrations are usually small or near zero. Thus, horizontal $NO_3^-$ gradients are much smaller than those of DIC. (At C4 there is a small advective import of $NO_3^-$, rather than the export that would be expected, because of non-homogeneities in $NO_3^-$ within the VICC.)

The biological uptake of carbon is closely balanced by the vertical flux at all stations except C4 where alongshore DIC import from the Juan de Fuca Strait is expected. Estimates of biological nitrogen uptake (using the Redfield C:N ratio) were larger than vertical fluxes at all stations, and an order of magnitude larger at C4 and C9. As seen in Fig. 9, the uptake of $NO_3^-$ appears to be

less than that predicted by the Redfield ratio on the C line so it is likely that the nitrogen uptake estimated in the budget is too high. After upwelling (G4, G6), however, when there was no evidence of excess biological carbon uptake (Fig. 9), nitrogen uptake was of the same order as the estimated vertical flux (Table 3).

In the daily budgets $CO_2$ gas flux is insignificant, though it is large after upwelling at G4 and is likely underestimated in the VICC as the only $pCO_2$ estimate available at C4 was from 10 m and was much lower than neighbouring surface values (Table 1). Estimated remineralization fluxes of both carbon and nitrogen are also small, but significant at the slope stations where PP was much lower and the system was closer to steady state.

## 4. Conclusions

The VICC is known to have a strong influence on PP over the shelf off southern Vancouver Island (Mackas et al., 1980; Crawford and Dewey, 1989). We show that the VICC has an equally strong influence on the inorganic carbon system. In this area, surface DIC is high, causing $pCO_2$ to exceed 1000 ppm. Gas evasion from the VICC could easily balance or exceed invasion over the outer shelf where biological drawdown is episodically high during the summer due to PP associated with upwelling events. It has been predicted that this biological drawdown of DIC could cause a large net invasion of $CO_2$ in coastal upwelling regions (Friederich et al., 1994). Although these periods of high $CO_2$ invasion occur, the $pCO_2$ of subsurface water over the shelf is high and when it is mixed into the surface at times of the year when PP is light limited, substantial gas evasion is likely and may balance summer invasion (*sensu* Ianson and Allen, 2002). Indeed, for conclusions to be drawn about net annual carbon fluxes in coastal upwelling regions seasonal measurements need to be made.

The high subsurface $pCO_2$ over the shelf is due to high DIC concentrations. These high concentrations are a result of exceptionally high PP, and particulate flux from surface waters (i.e. the 'biological pump' (Volk and Hoffert, 1985)), which is rapidly remineralized over the shelf in a small volume of water relative to the open ocean, thereby concentrating the remineralized DIC. In the open ocean deeper water that is enriched in DIC due to biological pumping is less likely to be mixed into the surface during the winter. Thus, the ability of coastal oceans to sequester atmospheric carbon should not be assumed and high coastal $f$-ratios should be interpreted with caution. Furthermore, the high DIC concentrations in the VICC, where biological production is high, were unexpected. The chemical concentrations in this current are unique due to intense mixing at its source. This enrichment introduces questions: What causes the ratio of inorganic C:N to be higher than in other parts of the ocean? What are the carbon dynamics in other coastal areas where mixing is intense?

The C:N ratio of biological uptake appears to be higher during the period of summer downwelling when nitrogen was limiting (exceeding the Redfield ratio), but close to the Redfield ratio following an upwelling event. Despite the excess carbon uptake at times, the POC:PON ratio remained relatively constant. We suggest that this excess carbon is excreted as DOC, as it is not incorporated into the phytoplankton. While excess carbon uptake does intensify surface $pCO_2$ drawdown its effect on biogeochemical nutrient cycling depends on the fate of this carbon. Our data do not suggest that a significant portion of organic matter exported from the euphotic zone is enriched in carbon. It is possible that some of the DOC that is produced is mixed out of the surface but the extent depends on the liability of this organic carbon as well as mixing dynamics.

It is well known that spatial and temporal inhomogeneities are large in coastal upwelling regions (e.g. Smith, 1994). Our data, gathered from one cruise, highlights this variability particularly in carbon. Advective effects cannot be ignored (e.g. Fig. 9) and the daily DIC budgets were far from steady state, dominated by cross-shore advection due to strong horizontal gradients in DIC over the shelf. Horizontal gradients in $NO_3^-$ were much smaller due to efficient biological uptake.

## Acknowledgements

We thank the officers and crew of the *CSS John P. Tully* and M. Davelaar and K. Johnson for their expertise and helpful guidance in the analysis and collection of total dissolved inorganic carbon and titration alkalinity samples. We are grateful to K. Hall, P. Harrison and D. Yelland for the use of their sampling bottles and to F. Whitney and S. Calvert for helpful discussions. We thank R. Thomson and J. Page for their assistance accessing data and G. Jackson for his patience while DI revised this manuscript. We appreciate the helpful comments of three anonymous reviewers and the editor. This study was funded by GLOBEC-Canada (supported by NSERC and Fisheries and Oceans, Canada) and by the NSERC Research grant program.

## References

Archer, D., 1995. Upper Ocean Physics as relevant to ecosystem dynamics: a tutorial. Ecosystem Applications 5, 724–739.

Carlson, C.A., Ducklow, H.W., 1995. Dissolved organic carbon in the upper ocean of the central equatorial Pacific Ocean, 1992: Daily and finescale vertical variations. Deep-Sea Research II 42, 639–656.

Carlson, C.A., Ducklow, H.W., Michaels, A.F., 1994. Annual flux of dissolved organic carbon from the euphotic zone in the northwestern Sargasso Sea. Nature 371, 405–408.

Christensen, J.P., 1994. Carbon export from continental shelves, denitrification and atmospheric carbon export. Continental Shelf Research 14, 547–576.

Codispoti, L.A., Friederich, G.E., Hood, D.W., 1986. Variability in the inorganic carbon system of the southeastern Bering Sea shelf during spring 1980 and spring–summer 1981. Continental Shelf Research 5, 133–160.

Crawford, W.R., Dewey, R.K., 1989. Turbulence and mixing: Sources of nutrients on the Vancouver Island continental shelf. Atmosphere-Ocean 27, 428–442.

Dickson, A.G., Goyet, C. (Eds.), DOE (U.S. Department of Energy), 1994. Handbook of methods for the analysis of the various parameters of the carbon dioxide system in seawater: Version 2.0, ORNL CDIAC-74.

Dugdale, R.C., Goering, J.J., 1967. Uptake of new and regenerated forms of nitrogen in primary productivity. Limnology and Oceanography 12, 196–206.

Dugdale, R.C., Wilkerson, F.P., Minas, H.J., 1995. The role of a silicate pump in driving new production. Deep-Sea Research I 42, 697–719.

Eppley, R.W., Peterson, B.J., 1979. Particulate organic matter flux and planktonic new production in the deep ocean. Nature 282, 677–680.

Faucher, M., Burrows, W.R., Pandolfo, L., 1999. Empirical-statistical reconstruction of surface marine winds along the western coast of Canada. Climate Research 11, 173–190.

Freeland, H.J., Denman, K.L., 1982. A topographically controlled upwelling center off southern Vancouver Island. Journal of Marine Research 40, 1069–1093.

Freeland, H.J., Crawford, W.R., Thomson, R.E., 1984. Currents along the Pacific coast of Canada. Atmosphere-Ocean 22, 151–172.

Friederich, G.E., Sakamoto, C.M., Pennington, J.T., Chavez, F.P., 1994. On the direction of the air–sea flux of $CO_2$ in coastal upwelling systems. In: Tsunogai, S., Iseki, K., Koike, I., Oba, T. (Eds.), Global Fluxes of Carbon and its Related Substances in the Coastal Sea-Ocean-Atmosphere System. Sapporo Hokkaido, Japan, IGBP, pp. 438–445.

Gargett, A.E., 1991. Physical processes and the maintenance of nutrient-rich euphotic zones. Limnology and Oceanography 36, 1527–1545.

Goldman, J.C., Hansell, D.A., Dennett, M.R., 1992. Chemical characterization of three large oceanic diatoms: potential impact on water column chemistry. Marine Ecology Progress Series 88, 257–270.

Harris, S., 2001. Size fractionated primary production and nutrient distribution on the west coast of Vancouver Island. M.Sc. Thesis, University of British Columbia Vancouver, Canada, 196pp.

Harrison, W.G., Platt, T., Lewis, M.R., 1987. $f$-ratio and its relationship to ambient nitrate concentration in coastal waters. Journal Plankton Research 9, 235–248.

Hickey, B., Thomson, R.E., Yih, H., LeBlond, P.H., 1991. Velocity and temperature fluctuations in a buoyancy-driven current off Vancouver Island. Journal of Geophysical Research 96, 10507–10538.

Hill, J.K., 1999. The distribution and partitioning of dissolved organic matter off the Oregon coast: a first look. Ph.D. Thesis, Oregon State University Corvallis, Oregon, 118pp.

Hsieh, W.W., Ware, D.W., Thomson, R.E., 1995. Wind-induced upwelling along the west coast of North America, 1899–1988. Canadian Journal of Fisheries and Aquatic Sciences 52, 325–334.

Hutchings, L., Pitcher, G.C., Probyn, T.A., Bailey, G.W., 1994. The chemical and biological consequences of coastal upwelling. In: Summerhayes, C.P., Emeis, K.-C., Angel, M.V., Smith, R.L., Zeitzschel, B. (Eds.), Upwelling in the Ocean: Modern Processes and Ancient Records. Wiley, New York, pp. 65–81.

Hutchins, D.A., Bruland, K.W., 1998. Iron-limited diatom growth and Si:N uptake ratios in a coastal upwelling regime. Nature 393, 561–564.

Ianson, D., Allen, S.E., 2002. A two-dimensional nitrogen and carbon flux model in a coastal upwelling region. Global Biogeochemical Cycles 16, (1):10.1029/2001GB001451.

Johnson, K.M., King, A.E., Sieburth, J.M., 1985. Coulometric $TCO_2$ analysis for marine studies; an introduction. Marine Chemistry 16, 61–82.

Johnson, K.M., Sieburth, J.M., Williams, P.J., Brandstromi, L., 1987. Coulometric total carbon dioxide analysis for marine studies; automation and calibration. Marine Chemistry 21, 117–133.

Johnson, K.S., Pytokowicz, R.M., Wong, C.S., 1979. Biological production and exchange of oxygen and carbon dioxide across the sea surface in Stuart Channel, British Columbia. Limnology and Oceanography 24, 474–482.

Kempe, S., Pegler, K., 1991. Sinks and sources of $CO_2$ in coastal seas: the North Sea. Tellus 43B, 224–235.

Large, W.G., Pond, S., 1981. Open ocean momentum flux measurements in moderate to strong winds. Journal of Physical Oceanography 11, 324–336.

Laws, E.A., Bannister, T.T., 1980. Nutrient and light-limited growth of *Thalassiosira fluviatilis* in continuous culture, with implications for phytoplankton growth in the ocean. Limnology and Oceanography 25, 457–473.

Lentz, S.J., 1992. The surface boundary layer in coastal upwelling regions. Journal of Physical Oceanography 22, 1517–1539.

Mackas, D.L., Louttet, G.C., Austin, M.J., 1980. Spatial distribution of zooplankton and phytoplankton off Vancouver Island. Canadian Journal of Aquatic Sciences 54, 2080–2096.

Millero, F.J., Poisson, A., 1981. International one-atmosphere equation of state for sea water. Deep-Sea Research 28, 625–629.

Millero, F.J., Lee, K., Roche, M., 1998. Distribution of alkalinity in the surface waters of the major oceans. Marine Chemistry 60, 111–130.

Millero, F.J., Shang, J.Z., Lee, K., Campbell, D.M., 1993. Titration alkalinity of seawater. Marine Chemistry 44, 153–165.

Milliman, J.D., 1993. Production and accumulation of calcium-carbonate in the ocean-budget of a nonsteady state. Global Biogeochemical Cycles 7, 927–957.

Parsons, T.R., Maita, Y., Lalli, C.M., 1984. A Manual of Chemical and Biological Methods for Seawater Analysis. Pergamon Press, Oxford, UK, 173pp.

Peña, M.A., Denman, K.L., Calvert, S.E., Thomson, R.E., Forbes, J.R., 1999. The seasonal cycle in sinking particle fluxes off Vancouver Island, British Columbia. Deep-Sea Research II 46, 2969–2992.

Press, W.H., Teukolsky, S.A., Vettering, W.T., Flannery, B.P., 1992. Numerical Recipes in C: the Art of Scientific Computing, 2nd Edition. Cambridge University Press, New York, USA, 994pp.

Redfield, A.C., Ketchum, B.H., Richards, F.A., 1963. The influence of organisms on the composition of sea-water. In: Hill, M.N. (Ed.), The Sea: Ideas and Observations on Progress in the Study of the Seas. Wiley, New York, pp. 26–77.

Richardson, T.L., Cullen, J.J., 1995. Changes in buoyancy and chemical composition during growth of a coastal marine diatom: ecological and biogeochemical consequences. Marine Ecology Progress Series 128, 77–90.

Sambrotto, R.N., Savidge, G., Robinson, C., Boyd, P., Takahashi, T., Karl, D.M., Langdon, C., Chipman, D., Marra, J., Codispoti, L., 1993. Elevated consumption of carbon relative to nitrogen in the surface ocean. Nature 363, 248–250.

Simpson, J.J., 1986. Processes affecting upper ocean chemical structure in an eastern boundary current. In: Burton, J.D., Brewer, P.G., Chesselet, R. (Eds.), Dynamic Processes in the Chemistry of the Upper Ocean. Plenum, New York.

Simpson, J.J., Zirino, A., 1980. Biological control of pH in the Peruvian coastal upwelling area. Deep-Sea Research 27, 733–744.

Skirrow, G., 1975. The dissolved gases—carbon dioxide. In: Riley, J.P., Skirrow, G. (Eds.), Chemical Oceanography. Vol. 2. Academic Press, London, pp. 1–192.

Smith, R.L., 1994. The physical processes of coastal ocean upwelling systems. In: Summerhayes, C.P., Emeis, K.-C., Angel, M.V., Smith, R.L., Zeitzschel, B. (Eds.), Upwelling in the Ocean: Modern Processes and Ancient Records. Wiley, New York, pp. 39–64.

Takahashi, T., Mathieu, G., Chipman, D.W., Goddard, J., Ma, L., 1991. Carbon dioxide in the surface water of the western equatorial Pacific Ocean. Final Technical Report to U.S. Department of Energy, 38pp.

Taylor, A.H., Geider, R.J., Gilbert, F.J., 1997. Seasonal and latitudinal dependencies of phytoplankton carbon-to-chlorophyll a ratios: results of a modelling study. Marine Ecology Progress Series 152, 51–66.

Thomson, R.E., Fine, I.V., 2003. Estimating mixed layer depth from oceanic profile data. Journal of Atmospheric and Oceanic Technology 20, 319–329.

Thomson, R.E., Hickey, B.M., LeBlond, P.H., 1989. The Vancouver Island coastal current: fisheries barrier and conduit. In: McFarlane, G.A. (Ed.),, Effects of Ocean Variability on Recruitment and an Evaluation of Parameters Used in Stock Assessment Models, Vol. 108. Canadian Special Publication of Fisheries and Aquatic Sciences, Ottawa, Canada, pp. 265–296.

Toth, D.J., Lerman, A., 1977. Organic matter reactivity and sedimentation rates in the ocean. American Journal of Science 277, 465–485.

Tsunogai, S., Watanabe, S., Sato, T., 1999. Is there a 'continental shelf pump' for the absorption of atmospheric $CO_2$? Tellus 51B, 701–712.

Verardo, D.J., Froelich, P.N., McIntyre, A., 1990. Determination of organic carbon and nitrogen in marine sediments using the Carlo Erba NA-1500 Analyzer. Deep-Sea Research 37, 157–165.

Volk, T., Hoffert, M.I., 1985. Ocean carbon pumps: analysis of relative strengths and efficiencies in ocean-driven atmospheric $pCO_2$ changes. In: Sundqvist, E.T., Broecker, W.S. (Eds.), The Carbon Cycle and Atmospheric $CO_2$, Natural Variations Archaen to Present AGU Monograph, No. 32. AGU, Washington, DC, pp. 99–110.

Wanninkhof, R., 1992. Relationship between gas exchange and wind speed over the ocean. Journal of Geophysical Research 97 (C5), 7373–7382.

Wanninkhof, R., Lewis, E., Feely, R.A., Millero, F.J., 1999. The optimal carbonate dissociation constants for determining surface water $pCO_2$ from alkalinity and total inorganic carbon. Marine Chemistry 65, 291–301.

Wong, C.S., Zhiming, Y., Johnson, W.K., Matear, R.J., Whitney, F.A., 1997. Dynamics and characterization of marine organic matter. In: Handa, N., Tanoue, E., Hama, T. (Eds.), Professor Handa's Retirement Commemorative Volume. Terra Scientific Publishing Company, Tokyo, pp. 107–116.

Wood, E.D., Armstrong, F.A.J., Richards, F.A., 1967. Determination of nitrate in seawater by cadmium-copper reduction to nitrite. Journal of the Marine Biological Association U.K. 47, 23–31.

Yool, A., Fasham, M.J.R., 2001. An examination of the "continental shelf pump" in an open ocean general circulation model. Global Biogeochemical Cycles 15, 831–844.